Available online at www.sciencedirect.com
SCIENCE DIRECT
Polymer 47 (2006) 3650–3660
polymer
www.elsevier.com/locate/polymer

Finite elasticity of thermoplastic elastomers

A.D. Drozdov *

Department of Chemical Engineering, Ben-Gurion University of the Negev, P.O. Box 653, Beer-Sheva 84105, Israel

Received 4 May 2005; received in revised form 8 March 2006; accepted 18 March 2006

Abstract

Strain energy density is developed for a network of flexible chains with weak excluded-volume interactions between segments. Constitutive equations (involving three to four material constants) are derived for an incompressible network of self-repellent chains at finite strains. These relations are applied to study the elastic response of thermoplastic elastomers at uniaxial tension. Good agreement is demonstrated between experimental data and results of numerical simulation at uniaxial deformations with elongation ratios up to 1100%.

Keywords: Thermoplastic elastomer; Excluded-volume interaction; Finite elasticity

1. Introduction

This study is concerned with modeling the mechanical response of thermoplastic elastomers at finite strains. Thermoplastic elastomers (TPE) are polymer materials that combine mechanical properties of vulcanized rubber (elastic recovery after large deformations) with high-speed processability and recyclability of thermoplastics [1]. Conventional TPEs are block copolymers made by copolymerization of two or more monomers by using block or graft polymerization techniques. Application of the block methods results in the formation of linear macromolecules consisting of alternating blocks of hard (crystallizable) and soft (amorphous) segments. Unlike vulcanized rubbers, where chains linked by chemical cross-links resist flow, TPEs demonstrate the mechanical behavior typical for polymer melts above the melting temperature for hard segments T_m. Below T_m, micro-phase separation occurs due to the thermodynamic incompatibility between blocks. When hard segments are not long enough to crystallize by the chain-folding process, bundling of hard segments occurs that induces formation of fringed micelles in a continuous amorphous phase [2]. These micelles serve as permanent cross-links that transmit forces between soft segments remaining in the rubbery state. As a result, in the interval of temperatures between the glass transition temperature for soft segments and the melting temperature for hard segments, the elastic response of TPEs resembles that of rubbers. Mechanical properties of thermoplastic elastomers has attracted substantial attention in the past 5 years. This may be explained by (i) development of novel classes of TPEs, (ii) discovery of new methods for their synthesis on the commercial scale, and (iii) introduction of new areas of application.

Experimental stress–strain curves of thermoplastic elastomers at uniaxial tension with large elongation ratios λ (up to $\lambda = 20$) demonstrate two qualitatively different types of stress–strain diagrams (Fig. 23 in [3]). The first is typical of rubber gum, whose stress–strain curve may be divided into three intervals: (i) in the first part, the engineering tensile stress σ strongly increases with λ at some initial interval ($1 < \lambda < 2$), after which (ii) the stress–strain curve changes its slope, and the stress weakly (sub-linearly) grows with elongation ratio in the region associated with an apparent softening ($2 < \lambda < 6$), and, finally, (iii) σ strongly (exponentially) increases with λ in the interval of deformations associated with strain-hardening ($\lambda > 6$). The other type of stress–strain dependencies is typical of bimodal networks [4] and semi-crystalline polymers [5]: the engineering stress (i) strongly increases at the initial stage of loading ($1 < \lambda < 2$), and (ii) grows linearly with λ after the slope of the stress–strain diagram changes. An increase in the network strength (driven, e.g. by the growth of the content of hard segments of chains) causes transformation of an 'elastic' stress–strain diagram (demonstrating a monotonous increase in the nominal stress with the nominal strain) into an 'elasto-plastic' curve with a pronounced yield point [6].

One of the first models for the elastic behavior of TPEs was proposed in [7] based on the slip-link theory [8]. Another model for the mechanical behavior of TPEs was proposed in

* Tel.: +972 8 6472146; fax: +972 8 6472916.
E-mail address: aleksey@bgumail.bgu.ac.il

0032-3861/$ - see front matter © 2006 Elsevier Ltd. All rights reserved.
doi:10.1016/j.polymer.2006.03.058

[9], where the finite extensibility of chains was accounted for by using a Pade approximation for the inverse Langevin function, whereas stress-induced rearrangement of internal structure of thermoplastic elastomers was treated with the help of a yield stress. Phenomenological stress–strain relations for rubbers and thermoplastic elastomers were suggested in [10]. In a series of papers [11–13], stress–strain relations were derived for the elasto-visco-plastic behavior of TPEs based on a Zener phenomenological model (an elastic spring connected in parallel with a Maxwell element).

A common feature of the above models is that they are grounded (explicitly or implicitly) on the assumption about finite extensibility of chains. Although this hypothesis seems natural at first sight, its implementation in terms of the James–Guth model [14] implies that polymer chains have also finite bending rigidity (a rigorous derivation of the Hamiltonian for a worm-like chain as a limit of a Hamiltonian for a discrete chain with correlated segments can be found in [15]). This makes the above approaches questionable, as no experimental evidence exists that thermoplastic elastomers are formed by semi-flexible chains.

It should be noted that finite extensibility is not the only reason for the non-Gaussian statistics of chains in a network. Among other reasons, one can mention the effect of excluded volume [16], as well as mechanically-induced changes in the distribution of lengths of chains in an ensemble.

Constitutive equations in finite elasticity of polymers based on the assumption that the average length of chains evolves under loading (in thermoplastic elastomers, this change may be attributed to stress-induced detachment of chains in the rubbery state from micelles formed by hard segments in the crystalline or glassy states) were developed in [17,18].

The objective of this study is to derive constitutive equations in finite elasticity of thermoplastic elastomers based on the concept of permanent networks of self-avoiding strands (the other physical hypothesis that leads to the non-Gaussian statistics of individual chains). Our aim is to develop stress–strain relations that (i) are based on a physically-plausible scenario for deformation at the micro-level, (ii) correctly describe available experimental data at uniaxial tension, (iii) involve a relatively small number of adjustable parameters that change consistently with physical characteristics of thermoplastic elastomers, and (iv) allow the above-described two types of the mechanical response of TPEs to be distinguished in terms of a single model.

The starting points of our analysis are (i) an explicit expression for the configurational free energy of a self-avoiding chain recently derived in [19] and (ii) the assumption that the strength of excluded-volume interactions between segments is affected by mechanical factors. The exposition is organized as follows. Configurational free energy of a self-repellent chain is calculated in Section 2. Strain energy density of a network of flexible chains with weak excluded-volume interactions is developed in Section 3. Constitutive equations are derived in Section 4. These relations are simplified for uniaxial tension of an incompressible network in Section 5. Adjustable parameters are found in Section 6 by fitting experimental data. Some concluding remarks are formulated in Section 7.

2. Flexible chains with excluded-volume interactions

A flexible chain is treated as a space curve with a contour length L. Its arbitrary configuration is described by $\mathbf{r}=\mathbf{r}(s)$, where $\mathbf{r}$ stands for the radius vector, and $s\in[0,L]$. The statistical weight of any configuration $\mathbf{r}(s)$ is determined by a Hamiltonian $H(\mathbf{r})$. The Hamiltonian of a standard Gaussian chain (no segment interactions) reads [16]

$$H_0(\mathbf{r}) = \frac{3k_BT}{2b}\int_0^L \left(\frac{d\mathbf{r}}{ds}(s)\right)^2 ds, \tag{1}$$

where k_B is Boltzmann's constant, T stands for the absolute temperature, b is the Kuhn length (the characteristic length of a segment), and the subscript index '0' refers to the Gaussian statistics. The Hamiltonian of a flexible chain with segment interactions is given by

$$H(\mathbf{r}) = H_0(\mathbf{r}) + \Phi(\mathbf{r}), \tag{2}$$

where Φ is the energy of intra-chain interactions. To describe excluded-volume interactions between segments, we accept the Edwards model [20], according to which Φ is proportional to the number of self-intersections

$$\Phi(\mathbf{r}) = \frac{vk_BTb^2}{2L}\int_0^L ds\int_0^L \rho(s-s')\delta\big(\mathbf{r}(s)-\mathbf{r}(s')\big)ds'. \tag{3}$$

Here $\delta(\mathbf{r})$ is the Dirac delta-function that counts intersections between segments labeled by s and s', the dot stands for inner product, v is a dimensionless coefficient that characterizes strength of self-avoiding interactions, the quantities b and L are introduced to preserve the correct dimensionality of the right-hand of Eq. (3), and $\rho(s)$ is a regularizing function that ensures that the average (over all configurations) number of self-intersections remains finite. This function ascribes to each intersection between segments labeled by s and s' some weight ρ that (i) equals zero when the difference $s-s'$ vanishes, and (ii) reaches its ultimate value of unity when the distance between these segments measured along the curve $\mathbf{r}(s)$ becomes relatively large. For definiteness, we set

$$\rho(s) = 1-\exp\left(-\frac{|s|}{l}\right), \tag{4}$$

where l is the characteristic length of internal inhomogeneity. Eq. (4) provides a smooth version of the Edwards regularization [20]

$$\rho(s) = 0 \quad (s<l), \qquad \rho(s) = 1 \quad (s>l),$$

with a cut-off length l. For a chain with a Hamiltonian $H(\mathbf{r})$, the distribution function $p(\mathbf{Q})$ of end-to-end vectors $\mathbf{Q}$ coincides

with the normalized Green function

$$p(\mathbf{Q}) = \int_{\mathbf{r}(0)=0}^{\mathbf{r}(L)=\mathbf{Q}} \exp\left(-\frac{H(\mathbf{r}(s))}{k_B T}\right) \mathcal{D}[\mathbf{r}(s)], \tag{5}$$

where the path integral with the measure $\mathcal{D}[\mathbf{r}]$ is calculated over all curves $\mathbf{r}(s)$ [15] that satisfy the boundary conditions $\mathbf{r}(0)=\mathbf{0}$ and $\mathbf{r}(L)=\mathbf{Q}$. The normalization condition for the Green function reads

$$\int p(\mathbf{Q}) \mathrm{d}\mathbf{Q} = 1, \tag{6}$$

where integration is performed over all vectors $\mathbf{Q}$.

Standard calculations of the distribution function for a Gaussian chain with Hamiltonian (1) result in

$$p_0(\mathbf{Q}) = \left(\frac{3}{2\pi B^2}\right)^{3/2} \exp\left(-\frac{3Q^2}{2B^2}\right), \tag{7}$$

where $B^2 = bL$ is the mean-square end-to-end distance. Omitting complicated transformations of the path integral in Eq. (5) [19], we present the final result in the following limit: (i) the strength of self-repellent interactions v tends to infinity, (ii) the ratio B/l that describes the internal inhomogeneity of segment interactions approaches zero, and (iii) their product remains finite

$$\frac{vB}{l} \to \left(\frac{2\pi}{3}\right)^{3/2} \chi, \tag{8}$$

where χ is an effective strength of excluded-volume interactions. Under condition (8), the distribution function for a chain with Hamiltonian (2)–(4) reads

$$p(\mathbf{Q}) = p_0(\mathbf{Q}) \left[1 - \frac{\chi}{4} \int_0^1 \exp\left(-\frac{3Q^2 x}{2B^2(1-x)}\right) E^{3/2}_{1/2,3/2} \left(-\chi\sqrt{x}(1-x)\right) \frac{\mathrm{d}x}{\sqrt{x(1-x)}}\right] \times \left[\frac{1}{\sqrt{\pi}} \int_0^1 E_{1/2,1/2}\left(-\chi\sqrt{x}(1-x)\right) \frac{\mathrm{d}x}{\sqrt{x(1-x)}}\right]^{-1}. \tag{9}$$

Here $E_{\alpha,\beta}(x)$ and $E^{\gamma}_{\alpha,\beta}(x)$ are the Mittag–Leffler functions [21]. These functions with half-integer indices in Eq. (9) are expressed by means of integrals of elementary functions

$$E^{3/2}_{1/2,3/2}(-x) = \frac{4}{\pi} \int_0^1 \left[\frac{1}{\sqrt{\pi}} - xz \exp(x^2 z^2) \mathrm{erfc}(xz)\right] \frac{\sqrt{z}\mathrm{d}z}{\sqrt{1-z}},$$

$$E_{1/2,1/2}(-x) = \frac{1}{\sqrt{\pi}} - x \exp(x^2) \mathrm{erfc}(x), \tag{10}$$

where

$$\mathrm{erfc}(x) = \frac{2}{\sqrt{\pi}} \int_x^\infty \exp(-t^2) \mathrm{d}t$$

is the complementary error function.

For a flexible chain with weak self-avoiding interactions ($\chi \ll 1$), we disregard terms beyond the first order of smallness in Eq. (10) and find that

$$p(\mathbf{Q}) = p_0(\mathbf{Q}) \left\{1 + \chi \left[\frac{2}{3} - \frac{1}{\sqrt{\pi}} \int_0^\infty \exp\left(-\frac{3Q^2 z^2}{2B^2}\right) \frac{\mathrm{d}z}{1+z^2}\right]\right\}. \tag{11}$$

The configurational free energy of a chain $\psi(\mathbf{Q})$ is calculated by means of the Boltzmann equation

$$\psi(\mathbf{Q}) = -k_B T \ln p(\mathbf{Q}). \tag{12}$$

Our aim now is to apply Eqs. (11) and (12) to find the strain energy of a weakly self-avoiding chain.

3. Strain energy density of a network of flexible chains

A thermoplastic elastomer is modeled as an incompressible network of flexible chains bridged by permanent junctions (micro-crystallite cross-linking points and entanglements between chains in the rubbery state) [9]. The network is treated as an ensemble of strands (segments of chains between consequent junctions). The position of any strand is entirely determined by its end-to-end vector (that is the positions of appropriate junctions). In the nonlinear elasticity theory, two states of a medium are conventionally distinguished [22]: (i) the reference (initial) state occupied before application of external loads, and (ii) the actual (deformed) state acquired after deformation. Denote by $\mathbf{Q}$ and $\mathbf{q}$ end-to-end vectors of a strand in the reference and actual states, respectively. Adopting the affinity hypothesis (which means that the deformation gradient for motion of junctions at the micro-level coincides with the deformation gradient $\mathbf{F}$ for macro-deformation), we write

$$\mathbf{q} = \mathbf{F} \cdot \mathbf{Q}. \tag{13}$$

Let $P(\mathbf{Q})$ be a distribution of end-to-end vectors $\mathbf{Q}$ of strands in the reference state of a network. An important difference between the present approach and the conventional theory of rubber elasticity is that we do not identify the distribution of end-to-end vectors in the network P (for a TPE, this distribution is of kinetic origin, because it depends on the rate of cooling of the melt) with the distribution of end-to-end vectors for a single chain p (which is characterized by the chain statistics).

It follows from Eqs. (12) and (13) that the increment (with respect to the actual state) of configurational free energy of a strand driven by deformation of the network reads

$$\Delta_1 \psi(\mathbf{F},\mathbf{q}) = \psi(\mathbf{Q}) - \psi(\mathbf{q}) = k_B T \left[\ln p(\mathbf{q}) - \ln p(\mathbf{F}^{-1} \cdot \mathbf{q})\right]. \tag{14}$$

Averaging Eq. (14) with the help of the distribution function $P(\mathbf{q})$ (the argument is the end-to-end vector in the actual state), we arrive at the formula for the strain energy

$$w_1(\mathbf{F}) = k_B T \int \left[\ln p(\mathbf{q}) - \ln p(\mathbf{F}^{-1}\cdot\mathbf{q})\right] P(\mathbf{q}) d\mathbf{q}. \quad (15)$$

By analogy with Eq. (14), we calculate the increment (with respect to the reference state) of configurational free energy

$$\Delta_2\psi(\mathbf{F},\mathbf{Q}) = \psi(\mathbf{q}) - \psi(\mathbf{Q}) = k_B T\left[\ln p(\mathbf{Q}) - \ln p(\mathbf{F}\cdot\mathbf{Q})\right].$$

Averaging this equality over the distribution of end-to-end vectors of strands in the network $P(\mathbf{Q})$ (the argument is the end-to-end vector in the reference state), we obtain

$$w_2(\mathbf{F}) = k_B T \int \left[\ln p(\mathbf{Q}) - \ln p(\mathbf{F}\cdot\mathbf{Q})\right] P(\mathbf{Q}) d\mathbf{Q}. \quad (16)$$

The strain energy per chain w is defined as the weighted sum of the strain energies w_1 and w_2 calculated by using two ways of averaging of the increment of configurational free energy

$$w = (1-a)w_1 + aw_2, \quad (17)$$

where $a \in [0,1]$ is a material parameter. Insertion of Eqs. (15) and (16) into Eq. (17) implies that

$$w = k_B T \int \left[a(\ln p(\mathbf{Q}) - \ln p(\mathbf{F}\cdot\mathbf{Q})) + (1-a)(\ln p(\mathbf{Q}) - \ln p(\mathbf{F}^{-1}\cdot\mathbf{Q}))\right] P(\mathbf{Q}) d\mathbf{Q}. \quad (18)$$

Assuming the functions $p(\mathbf{Q})$ and $P(\mathbf{Q})$ to be isotropic (spherically symmetric)

$$p(\mathbf{Q}) = p_*(Q^2), \qquad P(\mathbf{Q}) = P_*(Q^2), \quad (19)$$

where $p_*(r)$ and $P_*(r)$ are given functions of a scalar argument r, and $Q^2 = \mathbf{Q}\cdot\mathbf{Q}$, we arrive at the formula

$$w = k_B T \int \left[a \ln \frac{p_*(Q^2)}{p_*(\mathbf{Q}\cdot\mathbf{C}\cdot\mathbf{Q})} + (1-a)\ln \frac{p_*(Q^2)}{p_*(\mathbf{Q}\cdot\mathbf{C}^{-1}\cdot\mathbf{Q})}\right] P_*(Q^2) d\mathbf{Q}, \quad (20)$$

where the left and right Cauchy–Green deformation tensors are introduced by the conventional relations [22]

$$\mathbf{B} = \mathbf{F}\cdot\mathbf{F}^{T}, \qquad \mathbf{C} = \mathbf{F}^{T}\cdot\mathbf{F}, \quad (21)$$

where T stands for transpose.

Adopting the conventional assumption that the energy of inter-chain interactions is accounted for by means of the incompressibility condition [23], we calculate the strain energy density W per unit volume of a network as the sum of strain energies of individual strands

$$W = Mw$$

where M is the average number of strands per unit volume. Substituting Eq. (20) into this equality, we find the strain energy density of an incompressible isotropic polymer network:

$$W = k_B T M \int \left[a \ln \frac{p_*(Q^2)}{p_*(\mathbf{Q}\cdot\mathbf{C}\cdot\mathbf{Q})} + (1-a)\ln \frac{p_*(Q^2)}{p_*(\mathbf{Q}\cdot\mathbf{C}^{-1}\cdot\mathbf{Q})}\right] P_*(Q^2) d\mathbf{Q}. \quad (22)$$

3.1. Strain energy of a Gaussian strand in a network

Calculating the integral in Eq. (20) for an isotropic network of Gaussian chains with the distribution function of end-to-end vectors (7), we arrive at the Mooney–Rivlin formula

$$w = \mu_1(J_1 - 3) + \mu_2(J_2 - 3), \quad (23)$$

where

$$\mu_1 = \frac{2\pi a k_B T}{B^2} \int_0^\infty P_*(Q^2) Q^4 dQ,$$

$$\mu_2 = \frac{2\pi (1-a) k_B T}{B^2} \int_0^\infty P_*(Q^2) Q^4 dQ,$$

and J_m ($m = 1,2,3$) are principal invariants of the right Cauchy–Green tensor $\mathbf{C}$. In particular, at $a = 1$ (averaging of the increment of configurational free energy is performed over the distribution function of end-to-end vectors in the reference state), Eq. (23) implies the formula for the strain energy of a neo-Hookean elastic medium

$$w = \mu_1(J_1 - 3), \quad (24)$$

where

$$\mu_1 = \frac{2\pi k_B T}{B^2} \int_0^\infty P_*(Q^2) Q^4 dQ. \quad (25)$$

The following conclusions may be drawn: (i) the Mooney–Rivlin equation (23) is rigorously deduced within the classical theory of rubber elasticity, which implies that it is not a purely phenomenological relation, where the constant μ_2 characterizes 'deviations from the statistical theory' [24]; (ii) for an isotropic incompressible network of Gaussian strands, Eqs. (23) and (24) are valid for an arbitrary distribution function $P_*(r)$; and (iii) to develop the conventional relation for the elastic modulus

$$\mu_1 = \frac{1}{2} k_B T,$$

it suffices to presume the distribution of end-to-end vectors of strands in a network to be Gaussian

$$P(\mathbf{Q}) = \left(\frac{3}{2\pi B^2}\right)^{3/2} \exp\left(-\frac{3Q^2}{2B^2}\right), \quad (26)$$

substitute Eq. (26) into Eq. (25) and perform integration explicitly.

3.2. Strain energy of a weakly self-avoiding strand in a Gaussian network

Our aim now is to derive the strain energy of a weakly self-avoiding strand with the distribution function of end-to-end vectors (11) in an incompressible polymer network, where the distribution of end-to-end vectors of strands is given by Eq. (26). It is worth mentioning an important difference between a network of Gaussian strands (where segment interactions are disregarded) and a network of self-avoiding chains (where excluded-volume interactions are taken into account). The difficulty arising in the latter case is that the constitutive model should reflect not only interactions between segments belonging to the same strand (whose free energy is determined by Eqs. (11) and (12)), but also interactions between segments belonging to different strands located nearby. As the energy of excluded-volume interactions between segments belonging to different chains is unknown, we presume, in order to simplify the model, that the total configurational free energy of a strand in a network can be described by Eqs. (11) and (12) with χ treated as an average (over the network of strands) strength of excluded-volume interactions.

Based on this approximation, we find from Eqs. (11) to (20) that

$$w = \bar{w}_1 + \bar{w}_2, \tag{27}$$

where

$$\bar{w}_1 = k_B T \int \left[a \ln \frac{p_0(\mathbf{Q})}{p_0(\mathbf{Q}\cdot\mathbf{C}\cdot\mathbf{Q})} + (1-a)\ln \frac{p_0(\mathbf{Q})}{p_0(\mathbf{Q}\cdot\mathbf{C}^{-1}\cdot\mathbf{Q})} \right] P_*(Q^2)\mathrm{d}\mathbf{Q},$$

$$\begin{aligned}\bar{w}_2 = k_B T \int \Bigg\{ a \Bigg[&\ln\left(1+\chi\left(\frac{2}{3}-\frac{1}{\sqrt{\pi}}\int_0^\infty \exp\left(-\frac{3Q^2z^2}{2B^2}\right)\frac{\mathrm{d}z}{1+z^2}\right)\right) \\ &-\ln\left(1+\chi\left(\frac{2}{3}-\frac{1}{\sqrt{\pi}}\int_0^\infty \exp\left(-\frac{3(\mathbf{Q}\cdot\mathbf{C}\cdot\mathbf{Q})z^2}{2B^2}\right)\frac{\mathrm{d}z}{1+z^2}\right)\right)\Bigg] \\ +(1-a)\Bigg[&\ln\left(1+\chi\left(\frac{2}{3}-\frac{1}{\sqrt{\pi}}\int_0^\infty \exp\left(-\frac{3Q^2z^2}{2B^2}\right)\frac{\mathrm{d}z}{1+z^2}\right)\right) \\ &-\ln\left(1+\chi\left(\frac{2}{3}-\frac{1}{\sqrt{\pi}}\int_0^\infty \exp\left(-\frac{3(\mathbf{Q}\cdot\mathbf{C}^{-1}\cdot\mathbf{Q})z^2}{2B^2}\right)\right.\right. \\ &\left.\left.\frac{\mathrm{d}z}{1+z^2}\right)\right)\Bigg]\Bigg\} P_*(Q^2)\mathrm{d}\mathbf{Q}.\end{aligned} \tag{28}$$

The first expression in Eq. (28) is determined by Eq. (23)

$$\bar{w}_1 = \mu_1(J_1-3) + \mu_2(J_2-3). \tag{29}$$

Neglecting terms beyond the first order of smallness in the second equality in Eq. (28), using Eq. (26) and calculating the Gaussian integrals, we find that

$$\begin{aligned}\bar{w}_2 = \frac{\chi k_B T}{\sqrt{\pi}} \int_0^\infty \Bigg[&a\left(\frac{1}{\sqrt{(\lambda_1 z^2+1)(\lambda_2 z^2+1)(\lambda_3 z^2+1)}} - \frac{1}{\sqrt{(z^2+1)^3}}\right) \\ &+(1-a)\left(\frac{1}{\sqrt{\left(\lambda_1^{-1}z^2+1\right)\left(\lambda_2^{-1}z^2+1\right)\left(\lambda_3^{-1}z^2+1\right)}} - \frac{1}{\sqrt{(z^2+1)^3}}\right)\Bigg]\frac{\mathrm{d}z}{1+z^2}.\end{aligned} \tag{30}$$

Simple algebra implies that

$$(\lambda_1 z^2+1)(\lambda_2 z^2+1)(\lambda_3 z^2+1) = z^6 + J_2 z^4 + J_1 z^2 + 1,$$

$$\left(\lambda_1^{-1}z^2+1\right)\left(\lambda_2^{-1}z^2+1\right)\left(\lambda_3^{-1}z^2+1\right) = z^6 + J_1 z^4 + J_2 z^2 + 1,$$

where we utilized the incompressibility condition. Substitution of these expressions into Eq. (30) and use of Eqs. (27) and (29) results in

$$\begin{aligned}w = C_1^0\left[a(J_1-3)+(1-a)(J_2-3)\right] &+ C_2^0\chi\int_0^\infty \Bigg[a\left(\frac{1}{\sqrt{z^6+J_2z^4+J_1z^2+1}} - \frac{1}{\sqrt{(z^2+1)^3}}\right) \\ &+(1-a)\left(\frac{1}{\sqrt{z^6+J_1z^4+J_2z^2+1}} - \frac{1}{\sqrt{(z^2+1)^3}}\right)\Bigg]\frac{\mathrm{d}z}{1+z^2},\end{aligned} \tag{31}$$

where

$$C_1^0 = \frac{k_B T}{2}, \qquad C_2^0 = \frac{k_B T}{\sqrt{\pi}}.$$

Eq. (31) describes the strain energy of a weakly self-avoiding strand in a network. Multiplying Eq. (31) by the number of strands per unit volume M, we find the strain energy density per unit volume of an incompressible Gaussian network of self-avoiding chains,

$$\begin{aligned}W = C_1\left[a(J_1-3)+(1-a)(J_2-3)\right] &+ C_2\chi\int_0^\infty \Bigg[a\left(\frac{1}{\sqrt{z^6+J_2z^4+J_1z^2+1}} - \frac{1}{\sqrt{(z^2+1)^3}}\right) \\ &+(1-a)\left(\frac{1}{\sqrt{z^6+J_1z^4+J_2z^2+1}} - \frac{1}{\sqrt{(z^2+1)^3}}\right)\Bigg]\frac{\mathrm{d}z}{1+z^2},\end{aligned} \tag{32}$$

where

$$C_1 = C_1^0 M, \qquad C_2 = C_2^0 M.$$

The term in the first square brackets describes the strain energy of a Mooney–Rivlin medium. Bearing in mind that $J_1 \geq 3$ and $J_2 \geq 3$ for an arbitrary deformation of an incompressible medium, we infer that the other term in Eq. (32) is non-positive. This means that Eq. (32) determines a sub-linear (with respect to the principal invariants of the right Cauchy–Green tensor) strain energy density of a network, compared to the linear strain energy density provided by the Mooney–Rivlin formula (23). It is convenient to present Eq. (32) in the form

$$W = C_1 U_0 + C_2 \chi U_{\rm int}, \tag{33}$$

where the function

$$U_0 = a(J_1 - 3) + (1-a)(J_2 - 3) \tag{34}$$

is proportional to the strain energy of a Gaussian chain, whereas the function

$$U_{\rm int} = \int_0^\infty \left[a\left(\frac{1}{\sqrt{z^6 + J_2 z^4 + J_1 z^2 + 1}} - \frac{1}{\sqrt{(z^2+1)^3}} \right) + (1-a)\left(\frac{1}{\sqrt{z^6 + J_1 z^4 + J_2 z^2 + 1}} - \frac{1}{\sqrt{(z^2+1)^3}} \right) \right] \frac{{\rm d}z}{1+z^2} \tag{35}$$

is proportional to the increment of strain energy caused by excluded-volume interactions between segments.

4. Constitutive equations for a Gaussian network of self-avoiding chains

Eq. (32) demonstrates that the strain energy density W depends on the first two principal invariants, J_1 and J_2, of the right Cauchy–Green tensor $\mathbf{C}$ (the third principal invariant of this tensor equals unity for volume-preserving deformations). According to the Finger formula [22], the Cauchy stress tensor $\mathbf{\Sigma}$ is expressed in terms of W as

$$\mathbf{\Sigma} = -\varrho \mathbf{I} + 2(W_1 \mathbf{B} - W_2 \mathbf{B}^{-1}), \tag{36}$$

where ϱ stands for pressure, $\mathbf{I}$ is the unit tensor, and

$$W_m = \frac{\partial W}{\partial J_m} \qquad (m = 1,2).$$

Given a strain energy density W, Eq. (36) provides the stress–strain relation for an incompressible network of flexible strands. Adopting expression (32) for the strain energy density and differentiating this formula with respect to J_1 and J_2, we obtain

$$W_1 = \mu \left\{ a - \frac{\kappa}{2} \int_0^\infty \left[\frac{a}{(z^6 + J_2 z^4 + J_1 z^2 + 1)^{3/2}} + \frac{(1-a)z^2}{(z^6 + J_1 z^4 + J_2 z^2 + 1)^{3/2}} \right] \frac{z^2 {\rm d}z}{1+z^2} \right\},$$

$$W_2 = \mu \left\{ (1-a) - \frac{\kappa}{2} \int_0^\infty \left[\frac{a z^2}{(z^6 + J_2 z^4 + J_1 z^2 + 1)^{3/2}} + \frac{1-a}{(z^6 + J_1 z^4 + J_2 z^2 + 1)^{3/2}} \right] \frac{z^2 {\rm d}z}{1+z^2} \right\}, \tag{37}$$

where $\mu = C_1$ stands for an analog of the elastic modulus, and

$$\kappa = \frac{C_2 \chi}{C_1} = \frac{2\chi}{\sqrt{\pi}}$$

is proportional to the strength of excluded-volume interactions.

Until this point, all derivations were carried out within the classical statistical mechanics of flexible chains, and the only simplifications were (i) linearization (11) of the strain energy of a self-repellent chain under the assumption regarding the weakness of excluded-volume interactions, and (ii) account of excluded-volume interactions between segments belonging to neighboring strands with the help of an adjustable parameter χ in Eq. (11) for the strain energy of a single chain. As a result, we arrived at stress–strain relations (36) and (37) that involve three quantities reflecting the network properties at the micro-level: the elastic modulus μ (which is determined by temperature and concentration of strands in a network), the dimensionless ratio a (that describes the influence of statistics in the reference and deformed states on the configurational free energy), and the dimensionless coefficient κ (which is proportional to the average strength of segment interactions). The parameters μ and a are constant (independent of the applied deformation), whereas κ may be treated as a quantity affected by stresses (strains) that change the strength of segment interactions.

It seems natural to suppose that the average strength κ is reduced under active loading due to mechanically-induced orientation of strands and changes in the micro-structure of an elastomer. To describe evolution of κ with time t, the following first-order kinetic equation is suggested

$$\frac{{\rm d}\kappa}{{\rm d}t} = -\Gamma \kappa, \tag{38}$$

where Γ describes the rate of mechanically-induced decrease in the strength of excluded-volume interactions. As the present study focuses on the elastic response of TPEs, which means that time-dependent effects are disregarded, we suppose that Γ is proportional to the strain-rate intensity $D_{\rm i}$. For a three-dimensional deformation of an incompressible network, the strain-rate intensity reads

$$D_{\rm i} = \sqrt{\frac{2}{3} \mathbf{D}:\mathbf{D}}, \tag{39}$$

where $\mathbf{D}$ is the rate-of-strain tensor and the colon stands for convolution. To characterize the effect of mechanical factors on the rate of changes in the strength of interactions, we assume Γ to be proportional to the energy of segment interactions $U_{\rm int}$. Combining these hypotheses and using Eqs. (35) and (38), we

arrive at the formula

$$\frac{d\kappa}{dt} = \gamma D_i \kappa \int_0^\infty \left[a\left(\frac{1}{\sqrt{z^6 + J_2 z^4 + J_1 z^2 + 1}} - \frac{1}{\sqrt{(z^2+1)^3}} \right) + (1-a)\left(\frac{1}{\sqrt{z^6 + J_1 z^4 + J_2 z^2 + 1}} - \frac{1}{\sqrt{(z^2+1)^3}} \right) \right] \frac{dz}{1+z^2}, \quad \kappa(0) = \kappa_*, \tag{40}$$

where γ is a material constant. Eqs. (36), (37) and (40) provide a set of stress–strain relations for the elastic response of a thermoplastic elastomer modeled as an incompressible network of weakly self-avoiding chains. These equations involve four adjustable parameters, μ, a, γ, and κ_* to be found by fitting observations.

5. Uniaxial tension of an incompressible network

Our aim now is to simplify Eqs. (36), (37) and (40) for uniaxial tension of a permanent network. Uniaxial deformation of an incompressible bar is described by the formulas

$$x_1 = \lambda X_1, \qquad x_2 = \lambda^{-(1/2)} X_2, \qquad x_3 = \lambda^{-(1/2)} X_3,$$

where $\{X_m\}$ and $\{x_m\}$ are Cartesian coordinates in the reference and actual states, respectively, and λ denotes elongation ratio. The left and right Cauchy–Green tensors, $\mathbf{B}$ and $\mathbf{C}$, and the rate-of-strain tensor $\mathbf{D}$ are given by

$$\mathbf{B} = \mathbf{C} = \lambda^2 \mathbf{e}_1\mathbf{e}_1 + \lambda^{-1}(\mathbf{e}_2\mathbf{e}_2 + \mathbf{e}_3\mathbf{e}_3),$$
$$\mathbf{D} = \frac{\dot\lambda}{\lambda}\left[\mathbf{e}_1\mathbf{e}_1 - \frac{1}{2}(\mathbf{e}_2\mathbf{e}_2 + \mathbf{e}_3\mathbf{e}_3) \right], \tag{41}$$

where $\mathbf{e}_m$ are base vectors of the Cartesian frame in the reference state, and the superscript dot stands for the derivative with respect to time. Insertion of expressions (41) into Eq. (36) yields

$$\mathbf{\Sigma} = \Sigma_1 \mathbf{e}_1\mathbf{e}_1 + \Sigma_0(\mathbf{e}_2\mathbf{e}_2 + \mathbf{e}_3\mathbf{e}_3),$$

where

$$\Sigma_1 = -\varrho + 2(W_1\lambda^2 - W_2\lambda^{-2}),$$
$$\Sigma_0 = -\varrho + 2(W_1\lambda^{-1} - W_2\lambda). \tag{42}$$

Excluding ϱ from Eq. (42) and the boundary condition on the lateral surface of a specimen $\Sigma_0 = 0$ and introducing the engineering tensile stress $\sigma = \Sigma_1/\lambda$, we find that

$$\sigma = 2(W_1 + W_2\lambda^{-1})(\lambda - \lambda^{-2}). \tag{43}$$

It follows from Eqs. (39) and (41) that

$$J_1 = \lambda^2 + 2\lambda^{-1}, \qquad J_2 = 2\lambda + \lambda^{-2}, \qquad D_i = |\dot\lambda|\lambda^{-1}. \tag{44}$$

Substitution of these relations and Eq. (37) into Eq. (43) yields

$$\sigma(\lambda) = 2\mu\left(\lambda - \frac{1}{\lambda^2}\right)\left\{ \left(a + \frac{1-a}{\lambda}\right) - \frac{\kappa}{2\lambda}\int_0^\infty \left[\frac{a(z^2+\lambda)}{(z^6 + (2\lambda+\lambda^{-2})z^4 + (\lambda^2+2\lambda^{-1})z^2 + 1)^{3/2}} + \frac{(1-a)(\lambda z^2+1)}{\left(z^6 + (\lambda^2+2\lambda^{-1})z^4 + (2\lambda+\lambda^{-2})z^2 + 1\right)^{3/2}} \right] \frac{z^2 dz}{1+z^2} \right\}. \tag{45}$$

Insertion of expressions (44) into Eq. (40) implies that at active loading with $\dot\lambda > 0$

$$\frac{d\kappa}{d\lambda} = \gamma\frac{\kappa}{\lambda}\int_0^\infty \left[a\left(\frac{1}{\sqrt{z^6 + (2\lambda+\lambda^{-1})z^4 + (\lambda^2+2\lambda^{-1})z^2 + 1}} - \frac{1}{\sqrt{(z^2+1)^3}} \right) + (1-a)\left(\frac{1}{\sqrt{z^6 + (\lambda^2+2\lambda^{-1})z^4 + (2\lambda+\lambda^{-1})z^2 + 1}} - \frac{1}{\sqrt{(z^2+1)^3}} \right) \right] \frac{dz}{1+z^2}. \tag{46}$$

Eqs. (45) and (46) with the initial condition $\kappa(1) = \kappa_*$ provide a set of stress–strain relations for uniaxial tension of an incompressible network of weakly self-avoiding chains.

6. Comparison with observations

Eqs. (45) and (46) involve four material constants: (i) the elastic modulus μ, (ii) the average strength of excluded-volume interactions in the initial state κ_*, (iii) the rate of mechanically-induced changes in the strength of segment interactions γ, and (iv) the dimensionless ratio a that reflects correlations between the statistics of chains in the initial and current states.

To reduce the number of material constants and to distinguish between the rubber-like and yield-like responses of thermoplastic elastomers, we postulate that $a = 1$ for polymers demonstrating the rubber-like behavior (in accord with Eq. (17), this means that their strain energy is entirely determined by the statistics of strands in the initial state), whereas a is small compared with unity for polymers revealing the yield-like response (which means that their strain energy density is mainly determined by the statistics of strands in the current state). Our aim now is to find adjustable parameters in Eqs. (45) and (46) by fitting experimental data.

6.1. Rubber-like behavior

We begin with the analysis of polymers demonstrating the rubber-like elastic response, set $a = 1$ in the governing equations, and determine the constants κ_*, γ and μ by approximating observations.

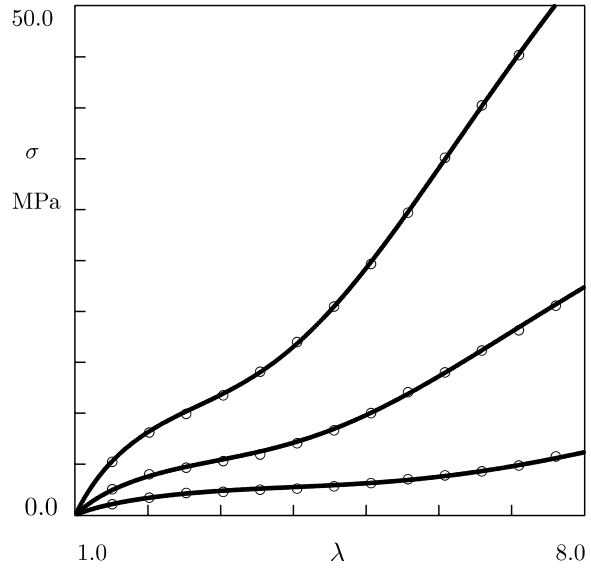

Fig. 1. The engineering tensile stress σ versus elongation ratio λ at uniaxial tension of TPUU. Circles: experimental data on TPUU prepared with 17.7, 18.8, and 26.9 g of HDMI, from bottom to top, respectively [25]. Solid lines: results of numerical simulation.

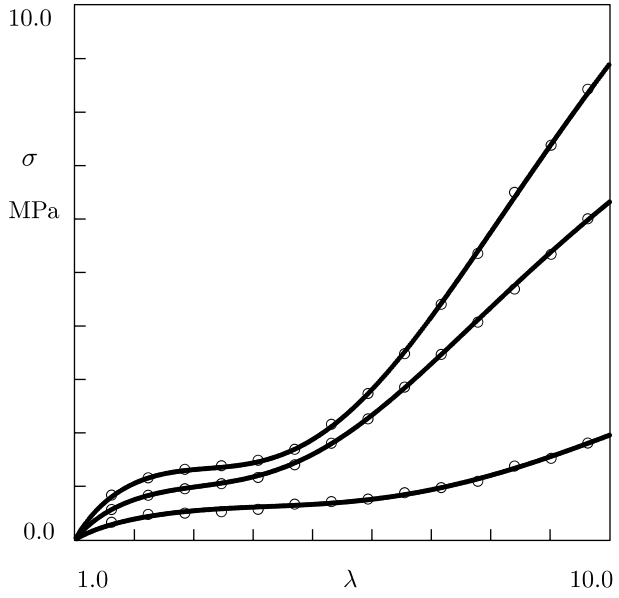

Fig. 2. The engineering tensile stress σ versus elongation ratio λ at uniaxial tension of PIB–PS. Circles: experimental data on PIB–PS prepared with 26.8, 30.7, and 33.8 wt% of PS, from bottom to top, respectively [26]. Solid lines: results of numerical simulation.

First, we fit the experimental data on hyper-branched segmented thermoplastic poly(urethane urea) elastomers (TPUU). For a detailed description of the synthesis and the experimental procedure, we refer to [25]. The dependencies of the engineering tensile stress σ on elongation ratio λ at uniaxial tension of TPUU with various contents of bis(4-isocyanotohexyl)methane (HDMI) are plotted in Fig. 1.

The following procedure is used to match the observations. We introduce some intervals $[0,\kappa_*^{\max}]$ and $[0,\gamma^{\max}]$, where the quantities κ_* and γ are assumed to be located, and divide these intervals by $J=10$ points $\kappa_*^{(i)}=i\Delta\kappa$ and $\gamma^{(j)}=j\Delta\gamma$ with $i,j=1,\ldots,J-1$, $\Delta\kappa=\kappa_*^{\max}/J$ and $\Delta\gamma=\gamma^{\max}/J$. For each pair $\{\kappa_*^{(i)},\gamma^{(j)}\}$, Eqs. (45) and (46) are solved numerically (by the Runge-Kutta method with the step $\Delta\lambda=10^{-3}$), and the modulus μ is found by the least-squares technique from the condition of minimum of the functional

$$\mathcal{F}=\sum_{\lambda_m}[\sigma^{\exp}(\lambda_m)-\sigma^{\mathrm{num}}(\lambda_m)]^2, \tag{47}$$

where $\sigma^{\exp}$ is the engineering tensile stress measured in the test, σ^{num} is given by Eq. (45), and the sum is performed over all elongation ratios λ_m at which the measurements are reported. The best-fit parameters $\kappa_*^{(i_0)}$ and $\gamma^{(j_0)}$ are determined by minimizing the functional (47) on the set $\{\kappa_*^{(i)},\gamma^{(j)}\}$. Afterwards, the same procedure is repeated several times for the new intervals $[\kappa_*^{(i_0)}-\Delta\kappa,\kappa_*^{(i_0)}+\Delta\kappa]$ and $[\gamma^{(j_0)}-\Delta\gamma,\gamma^{(j_0)}+\Delta\gamma]$ to ensure an acceptable accuracy of matching the data. Approximation of observations is carried out for each stress–strain curve separately.

The results of numerical simulation are depicted in Fig. 1, and the best-fit parameters μ, κ_* and γ are listed in Table 1. Fig. 1 demonstrates excellent agreement between the experimental data and the results of numerical analysis at elongation ratios up to $\lambda=8$. According to Table 1, all material constants increase with content of HDMI, that is with concentration of hard segments, which appears to be physically plausible. It should be noted that μ in Eq. (45) serves as an average elastic modulus of an elastomer, and it does not necessary coincide with the Young's modulus measured at small strains.

We proceed with matching observations in uniaxial tensile tests on polystyrene–polyisobutylene–polystyrene (PIB–PS) triblock copolymers with various contents of polystyrene (PS). A detailed description of TPEs and the experimental procedure is reported in [26]. The experimental stress–strain curves are depicted in Fig. 2 together with their approximations by the model. Adjustable parameters in Eqs. (45) and (46) found by using the above-described algorithm are given in Table 2. Fig. 2 demonstrates good agreement between the observations and the results of numerical simulation. According to Table 2, the material parameters μ, κ_* and γ change consistently with the content of polystyrene (the only exception is the value of γ at the maximal content of PS).

Table 1
Adjustable parameters for TPUU with various contents of HMDI

HMDI (g)	μ (MPa)	κ_*	γ
17.0	0.63	0.069	1.3
18.8	1.55	0.090	2.5
26.9	3.54	0.103	3.1

Table 2
Adjustable parameters for PIB–PS block copolymers with various contents of PS

PS (wt%)	μ (MPa)	κ_*	γ
26.8	0.15	0.069	1.14
30.7	0.34	0.108	2.12
33.8	0.50	0.116	1.92

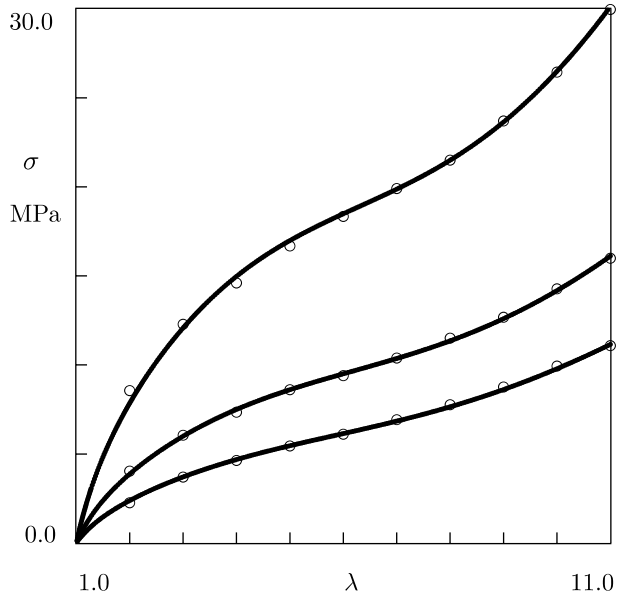

Fig. 3. The engineering stress σ versus elongation ratio λ at uniaxial tension of PEBAX films. Circles: experimental data on PEBAX with 11.9, 13.0 and 27.2 mol% of PA, from bottom to top, respectively [6]. Solid lines: results of numerical simulation.

We now approximate experimental data at uniaxial tension of commercial thermoplastic elastomers PEBAX [poly(ether-*block*-amide)] with various concentrations of polyamide (PA). For a description of the material properties and the experimental procedure, see [6]. The observations in tensile tests are depicted in Fig. 3 together with their fits by the model. Material constants are determined by the algorithm described above and are presented in Table 3. Fig. 3 reveals excellent agreement between the experimental data at elongations up to $\lambda = 11$ and the results of numerical analysis. Table 3 shows that the adjustable parameters in Eqs. (45) and (46) are affected by the concentration of PA in a consistent way.

The following conclusions may be drawn from the results presented in Tables 1–3:

1. The elastic modulus of thermoplastic elastomers μ grows with content of rigid phase, but this increase does not obey the standard rule of mixture.
2. The initial strength of excluded-volume interactions κ_* grows with concentration of rigid phase. The increase in κ_* is pronounced for TPEs where hard segments form micro-domains in the glassy state (Tables 1 and 2), whereas it is rather weak or it even disappears entirely for TPEs with crystallizable segments (Table 3).
3. The rate of decrease in strength of excluded-volume interactions γ strongly grows with content of rigid phase for TPEs with glassy micro-domains and weakly decays for TPEs with crystalizable hard segments.

Table 3
Adjustable parameters for PEBAX with various contents of PA

PA (mol%)	μ (MPa)	κ_*	γ
11.9	0.75	0.027	0.66
13.0	1.23	0.029	0.60
27.2	2.52	0.031	0.58

The increase in the elastic modulus μ with concentration of rigid phase appears to be natural due to the difference in moduli of hard and soft micro-domains. The strong growth of κ_* and γ with content of rigid phase for TPEs with hard segments forming glassy micro-domains (TPUU and PIB–PS) may be attributed to mechanically-induced changes in the molecular architecture in the rubbery phase with no rearrangement of rigid micro-domains. On the contrary, the weak decrease in γ with content of rigid phase (PEBAX) may be explained by screening of such a dependence driven by transformations of micro-crystallites. Although this statement requires additional investigations, some validation of this hypothesis is provided by comparison of the characteristic size of rigid micro-domains in the glassy state (1–2 nm [27]) with that in the crystalline state (16–19 nm [6]).

6.2. Yield-like behavior

Our aim now is to approximate stress–strain diagrams at uniaxial tension of TPEs revealing the yield-like response. Unlike thermoplastic elastomers demonstrating the rubber-like behavior, we fit observations with the help of four adjustable parameters: μ, κ_*, γ and a. The algorithm of matching experimental data is similar to that employed in the previous section. The only difference is that we divide the intervals where κ_*, γ and a are assumed to be located by points $\kappa_*^{(i)}$, $\gamma^{(j)}$ and $a^{(k)}$. For each triple $\{\kappa_*^{(i)},\gamma^{(j)},a^{(k)}\}$, we solve Eqs. (45) and (46) numerically, find the elastic modulus μ by using the least-squares technique from the condition of minimum of the functional (47), and choose the best-fit values of the material constants by minimizing $\mathcal{F}$ in Eq. (47).

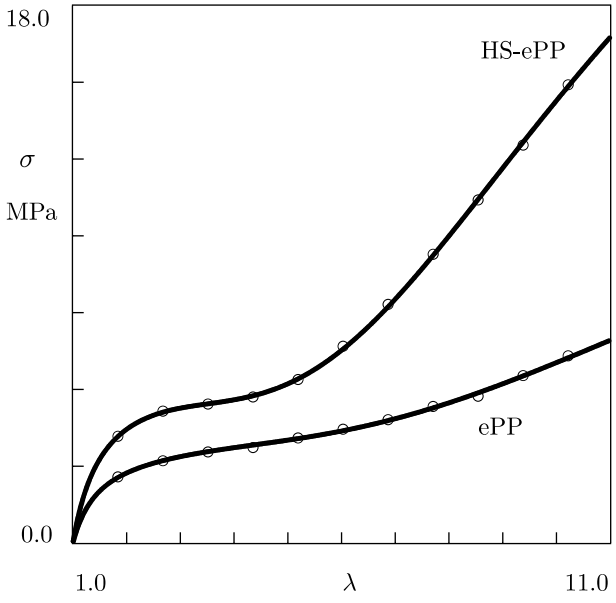

Fig. 4. The engineering stress σ versus elongation ratio λ at uniaxial tension of elastomeric polypropylene (ePP) and its heptane-soluble fraction (HS–ePP). Circles: experimental data [28]. Solid lines: results of numerical simulation.

Table 4
Adjustable parameters for elastomeric polypropylene with various amounts of isotactic pentads IP and mass average molecular weights M_w

Polymer	IP (%)	M_w (kg/mol)	μ (MPa)	κ_*	γ	a
ePP	34	200.1	1.16	0.012	1.4	0.24
HS–ePP	44	220.8	1.96	0.038	2.0	0.37

We begin with matching stress–strain dependencies at uniaxial tension of elastomeric polypropylene (ePP) [polypropylene (PP) whose chains are composed of isotactic (crystalizable) and atactic (amorphous) segments] reported in [28]. For a detailed description of synthesis and the experimental procedure, the reader is referred to [28]. The experimental stress–strain diagrams of ePP and its heptane-soluble fraction (HS–ePP) are depicted in Fig. 4 together with their approximations by the model. The best-fit parameters in the constitutive equations are listed in Table 4. Fig. 4 demonstrates excellent quality of fitting observations at elongation ratios up to $\lambda = 11$. According to Table 4, where the content of isotactic pentads (IP) is provided, the quantities μ, κ_*, γ and a noticeably increase with the degree of crystallinity and mass-average molecular weight M_w.

We proceed with the approximation of experimental data at uniaxial tension of elastomeric polypropylenes with various mass-average molecular weights M_w and polydispersity indices (PDI). For a description of synthesis of ePP and the experimental procedure, see [29]. The experimental stress–strain diagrams are depicted in Fig. 5 together with their fits by the model. This figure shows good agreement between the observations and the results of numerical simulation. The best-fit values of the adjustable parameters in the constitutive equations are listed in Table 5. According to this table, the elastic modulus μ and the rate of mechanically-induced

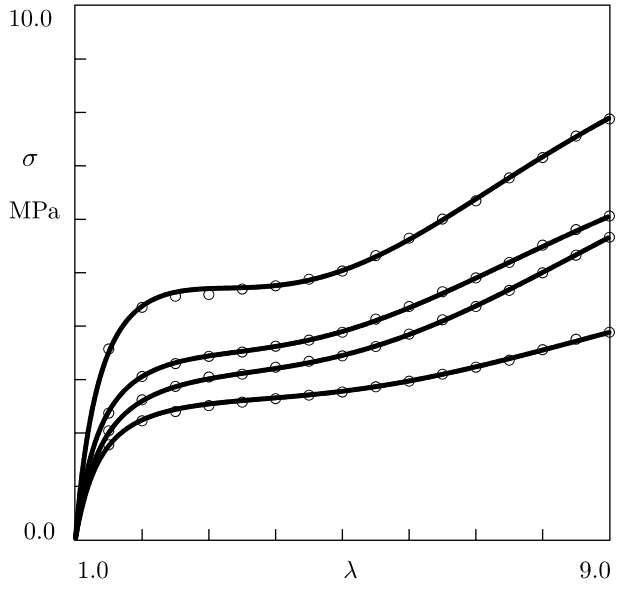

Fig. 5. The engineering stress σ versus elongation ratio λ at uniaxial tension of elastomeric polypropylene (ePP). Circles: experimental data on specimens with the weight-average molecular weight 214.0, 395.0, 386.0, and 293.0, from bottom to top, respectively [29]. Solid lines: results of numerical simulation.

Table 5
Adjustable parameters for elastomeric polypropylene with various contents of isotactic pentads (IP), mass-average molecular weights M_w and polydispersity indices (PDI)

IP (%)	M_w (kg/mol)	PDI	μ (MPa)	κ_*	γ	a
32.9	214.0	2.70	1.24	0.008	2.2	0.09
33.8	395.0	2.60	1.39	0.014	2.2	0.16
37.0	386.0	2.84	1.71	0.013	2.8	0.11
42.7	293.0	4.29	2.57	0.016	3.0	0.08

changes in strength of segment interactions γ are strongly affected by the degree of crystallinity, and they noticeably grow with content of isotactic pentads IP. The initial strength of excluded-volume interactions κ_* increases with degree of crystallinity as well, but it is also influenced by molecular weight M_w. On the contrary, the parameter a (reflecting the statistics of strands in the reference and current states) is mainly affected by molecular weight and polydispersity index. It should be noted, however, that although within each set of observations plotted in Figs. 4 and 5, the parameters μ and γ are mainly affected by the concentration of isotactic pentads, the effect of IP is different for ePPs prepared by different research groups. The latter means that the conditions of synthesis noticeably affect the material constants in the constitutive equations.

The following conclusions are drawn:

1. Unlike TPEs revealing the rubber-like mechanical response, for which the parameter a equals unity, this quantity ranges from 0.1 to 0.4 for thermoplastic elastomers demonstrating the yield-like behavior.
2. The elastic modulus of TPEs μ is mainly affected by the degree of crystallinity, while the influence of molecular weight and polydispersity index on this parameter is weak.
3. The initial strength of excluded-volume interactions κ_* and the rate of mechanically-induced decrease in strength of segment interactions γ accept similar values for TPEs showing the rubber-like and yield-like behavior.

7. Concluding remarks

Constitutive Eqs. (36), (37) and (40) have been derived for the elastic response of thermoplastic elastomers at finite strains. Unlike conventional theories of rubber elasticity that disregard segment interactions, the stress–strain relations take into account excluded-volume interactions between segments of flexible chains. The model is based on the following hypotheses: (i) an elastomer is thought of as an incompressible network of chains bridged by permanent junctions; (ii) micro-deformation of strands coincides with macro-deformation of the network; (iii) an arbitrary strand is treated as a self-avoiding chain with an effective strength that accounts for excluded-volume interactions between segments belonging to the same strand, as well as between segments belonging to different strands, (iv) the strength of excluded-volume interactions is strongly affected by mechanical deformations, its evolution

under loading is described by the first-order kinetic equation (40), (v) the strain energy density of an incompressible network equals the sum of strain energies of individual strands, (vi) the distribution function of distances between junctions in the reference (undeformed) state of the network is Gaussian. The assumptions (i), (ii) (v) and (vi) are typical of conventional models in rubber elasticity, whereas hypotheses (iii) and (iv) are novel.

The stress–strain relations have been simplified for uniaxial tension of an incompressible network, see Eqs. (45) and (46), and have been applied to approximate experimental data. It is demonstrated that (i) the constitutive model correctly describes experimental data at uniaxial tension of thermoplastic elastomers with elongation ratios up to 1100%, (ii) it distinguishes between the rubber-like and yield-like responses of TPEs, and (iii) its material parameters are affected by the micro-structure of thermoplastic elastomers in a physically plausible way. An advantage of Eqs. (45) and (46) is that (i) they are 'physically motivated' in the sense that these relations are developed based on a simple physical picture on the micro-level, (ii) they contain only three to four adjustable parameters that have transparent physical meaning and can be found by fitting observations in standard mechanical tests.

References

[1] Holden G, Kricheldorf HR, Quirk PR, editors. Thermoplastic elastomers. 3rd ed. Munich: Hanser/Gardner Publishers; 2004.
[2] Bensason S, Minick J, Moet A, Chum S, Hiltner A, Baer E. J Polym Sci, Part B: Polym Phys 1996;34:1301–15.
[3] Müller G, Rieger B. Prog Polym Sci 2002;27:815–51.
[4] Mark JE. Macromol Symp 2003;201:77–83.
[5] Drozdov AD, Christiansen J de C. Int J Solids Struct 2003;40:1337–67.
[6] Sheth JP, Xu J, Wilkes GL. Polymer 2003;44:743–56.
[7] Bensason S, Stepanov EV, Chum S, Hiltner A, Baer E. Macromolecules 1997;30:2436–44.
[8] Ball RC, Doi M, Edwards SF, Warner M. Polymer 1981;22:1010–8.
[9] Haward RN. Polymer 1999;40:5821–32.
[10] Lambert-Diani J, Rey C. Eur J Mech A/Solids 1999;18:1027–43.
[11] Boyce MC, Kear K, Socrate S, Shaw K. J Mech Phys Solids 2001;49: 1073–98.
[12] Boyce MC, Socrate S, Kear K, Yeh O, Shaw K. J Mech Phys Solids 2001; 49:1323–42.
[13] Qi HJ, Boyce MC. Mech Mater 2005;52:2187–205.
[14] James HM, Guth E. J Chem Phys 1943;11:455–81.
[15] Kleinert H. Path integrals in quantum mechanics, statistics, and polymer physics. Singapore: World Scientific; 1995.
[16] Doi M, Edwards SF. The theory of polymer dynamics. Oxford: Clarendon Press; 1986.
[17] Drozdov AD. Polym Bull 2001;46:215–22.
[18] Drozdov AD, Dorfmann A. Continuum Mech Thermodyn 2001;13: 395–417.
[19] Drozdov AD. Macromol Theory Simul. in press.
[20] Edwards SF. Proc Phys Soc (London) 1965;85:613–24.
[21] Erdelyi A, editor. Higher transcendental functions, vol. 3. New York: McGraw-Hill; 1953.
[22] Drozdov AD. Finite elasticity and viscoelasticity. Singapore: World Scientific; 1996.
[23] Treloar LRG. The physics of rubber elasticity. Oxford: Clarendon Press; 1975.
[24] Yeoh OH, Fleming PD. J Polym Sci, Part B: Polym Phys 1997;35: 1919–31.
[25] Unal S, Yilgor I, Yilgor E, Sheth JP, Wilkes GL, Long TE. Macromolecules 2004;37:7081–4.
[26] Antony P, Puskas JE, Kontopoulou M. Polym Eng Sci 2003;43:243–53.
[27] Musselman SG, Santosusso TM, Barnes JD, Sperling LH. J Polym Sci, Part B: Polym Phys 1999;37:2586–600.
[28] Wiyatno W, Fuller GG, Pople JA, Gast AP, Chen Z-R, Waymouth RM, et al. Macromolecules 2003;36:1178–87.
[29] Rajan GS, Vu YT, Mark JE, Mayers CL. Eur Polym J 2004;40:63–71.